Energy and Buildings 75 (2014) 290–300

Contents lists available at ScienceDirect

Energy and Buildings

journal homepage: www.elsevier.com/locate/enbuild

Experimental analysis of a direct expansion geothermal heat pump in heating mode

Jean-Louis Fannou*, Clément Rousseau, Louis Lamarche, Kajl Stanislaw

Thermal Technology Center (TTC), Department of Mechanical Engineering, École de technologie supérieure, Université du Québec, 1100, Notre-Dame Street West, Montreal H3C 1K3, Canada

ARTICLE INFO

Article history:
Received 23 August 2013
Received in revised form 9 February 2014
Accepted 12 February 2014

Keywords:
Geothermal
Heat pump
Direct expansion (DX)
Heating capacity
Heat extraction rate
Coefficient of performance
Electricity

ABSTRACT

In this study, we present an experimental analysis of a direct expansion (DX) geothermal heat pump (GHP) installed in the Thermal Technology Center (TTC) of the École de technologie supérieure in Montreal. The residential heating system studied consists of three geothermal 30 m deep wells, which use R22 as refrigerant. During the test campaign, which ran over a one-month period in early spring, the coefficient of performance of the heat pump varied between 2.70 and 3.44, with a daily average of 2.87. The heating capacity reached a daily average of 8.04 kW, for a cooling water constant volumetric flow rate of 0.38 L s^{-1}. The mean the ground heat extraction rate from was 58.2 W m^{-1}. The tests performed helped to highlight a pressure drop coupled with a relatively large superheating revealing a flow rate mal-distribution in geothermal evaporators. The effects of some factors (condenser cooling water inlet temperature, condensing temperature, pressure drop in the evaporator, thermal properties of soil and grout) that affect DX system performance are also presented. Finally, a comparative study between the use of electricity and the DX heat pump as home heating source shows that the DX heat pump provides savings of approximately 70% over the electricity.

1. Introduction

The last decade has seen renewed interest in Geothermal Heat Pumps (GHP) [1] not only because of energy scarcity and increasing demand [2,3], but also for the performance and cost savings they provide with long-term use [4–6]. In general, geothermal heat pumps available in the market are secondary loop (SL) systems (Fig. 1) and present certain advantages over their air-to-air counterparts, including low power consumption (43.17% less in heating and 37.18% less in cooling [7]), no influence of outside temperature on performance, low maintenance costs associated with failure due to their exposure to weather elements, and their use of a power source (ground) at a relatively constant temperature throughout the year [8]. Their main drawback however, is their very high initial investment cost compared to air-to-air systems [9]. To achieve even more savings on investment costs, another type of heat pump eliminates ground loop on its secondary side; it is classified under direct expansion geothermal heat pumps (DX GHP) because it has the characteristic of having one of its components buried in the soil and acting as a condenser or evaporator depending on the operation mode (Fig. 2). Compared to secondary loop geothermal systems, this system presents the following advantages [10]:

- Reduced costs by eliminating the secondary loop ground side: no heat exchanger or pump (Fig. 2)
- Low power consumption for operation
- Reduced maintenance costs
- Improved heat transfer conditions between the grout and the U-tube thanks to copper (high thermal conductivity) used to manufacture the underground U-tube compared to plastic used in secondary loop systems

Despite these advantages, DX systems have largely remained at the experimental stage because for many years, researchers and the scientific community have focused their research more on secondary loop systems, as well as because of some problems encountered with DX systems: oil return, problem of starting the compressor, and the possibility of pollution due of important refrigerant quantity [2,11,12].

* Corresponding author at: Mechanical Engineering Department, École de technologie supérieure, 1125 William Street, Montreal H3C 1P7, Canada.
Tel.: +1 514 396 8858.
E-mail addresses: jean-louis.fannou.1@ens.etsmtl.ca (J.-L. Fannou), clement.rousseau.2@ens.etsmtl.ca (C. Rousseau), louis.lamarche@etsmtl.ca (L. Lamarche), stanislaw.kajl@etsmtl.ca (K. Stanislaw).

http://dx.doi.org/10.1016/j.enbuild.2014.02.026
0378-7788/

Nomenclature

COP_{sys}	coefficient of performance of the system
COP_{hp}	coefficient of performance of the heat pump
COP	coefficient of performance
T_{w_in}	condenser water inlet temperature (°C)
T_{cd}	condensing temperature (°C)
T_{w_out}	outlet temperature of the condenser water (°C)
Cp_w	heat capacity of water (kJ/kg K)
$\dot{m}_w$	cooling water flow rate to the condenser (kg/s)
W_{comp}	Power input to the compressor (kW)
Q_H	heating capacity (KW)
H	deep well (m)
q	ground heat extraction rate ($W\,m^{-1}$)
T_1_L	refrigerant temperature at the inlet of the borehole #1 (°C)
T_2_L	refrigerant temperature at the inlet of the borehole #2 (°C)
T_3_L	refrigerant temperature at the inlet of the borehole #3 (°C)
T_1_V	refrigerant temperature at the outlet of the borehole #1 (°C)
T_2_V	refrigerant temperature at the outlet of the borehole #2 (°C)
$T_3 - V$	refrigerant temperature at the outlet of the borehole #3 (°C)
P_1_L	refrigerant pressure at the inlet of the borehole #1 (kPa)
P_2_L	refrigerant pressure at the inlet of the borehole #2 (kPa)
P_3_L	refrigerant pressure at the inlet of the borehole #3 (kPa)
P_1_V	refrigerant pressure at the outlet of the borehole #1 (kPa)
P_2_V	refrigerant pressure at the outlet of the borehole #2 (kPa)
P_3_V	refrigerant pressure at the outlet of the borehole #3 (kPa)
SL	secondary loop
GHP	geothermal heat pump
DX	direct expansion
hp	heat pump

A review of the literature reveals the presence of several publications on geothermal secondary loop systems [3,8,13], but a lack of scientific research and publications on direct expansion geothermal heat pump systems [14,15]. However, over the past decade, some works have surfaced on DX heat pumps. Wang X. et al. [16] conducted an experimental study of a DX heat pump with R134a in heating mode. The system consisted of three vertical 30 m deep boreholes examined over a period of 20 days in the winter. According to the results, on average, COP_{hp} and COP_{sys} were 3.55 and 2.28, respectively, and the average heating capacity obtained was 6.43 kW. They highlighted the problem of mal-distribution of refrigerant flow in the evaporator. Wang H. et al. [17] conducted an experimental study on a DX heat pump in heating mode, consisting of four vertical 20 m wells for which a copper coil system was developed to facilitate oil return. The heating capacity reached 6.41 kW with COP_{hp} and COP_{sys} average of 3.12 and 2.88, respectively. A techno-economic study was carried out by Guo Y. et al. [2] comparing DX systems with SL systems in cooling mode. They concluded that DX systems are more efficient and more economical than SL systems. In addition, they posited that DX systems are put forward in the industry if the problem of oil return is satisfactorily

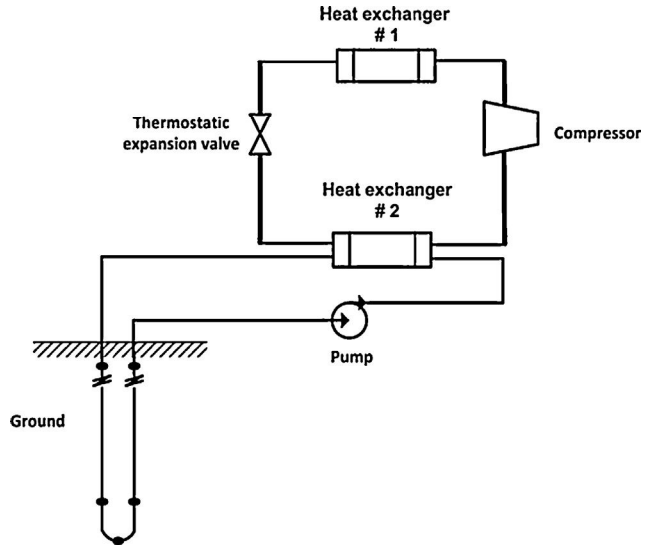

Fig. 1. Schematic of a traditional secondary loop geothermal heat pump.

resolved. Austin and Sumathy [18] conducted a parametric study on the performance of a CO_2 DX heat pump in a transcritical cycle. A numerical model was developed and optimized parameters of the heat pump improved the performance by 18% as compared to the reference model. Rousseau et al. [19] modeled a DX evaporator in a Comsol Multiphysics software environment in heating mode. The model obtained was validated experimentally. Patrick J. Hughes [15], in his diagnosis of the obstacles to the use of geothermal system, noticed a limitation to the lack of infrastructure facility, technology and technique for understanding geothermal systems.

Our study has the following technological features:

- Configuration of ground loops: the boreholes #2 and 3 were inclined while borehole #1 remained vertical (Fig. 3). This configuration has the advantage of reducing the distance between the wells, promoting its installation in residential homes. For vertical boreholes, Mei et al. and Wang et al. [11,17] recommended a depth of 4 to 6 m. In addition, the configuration used for boreholes #2 and 3 reduces the gravitational force needed to climb the refrigerant through the evaporators.

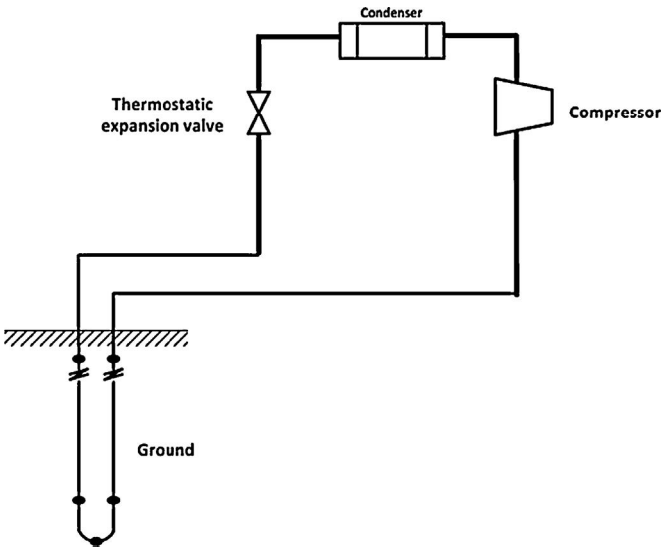

Fig. 2. Schematic of a direct expansion geothermal heat pump (DX).

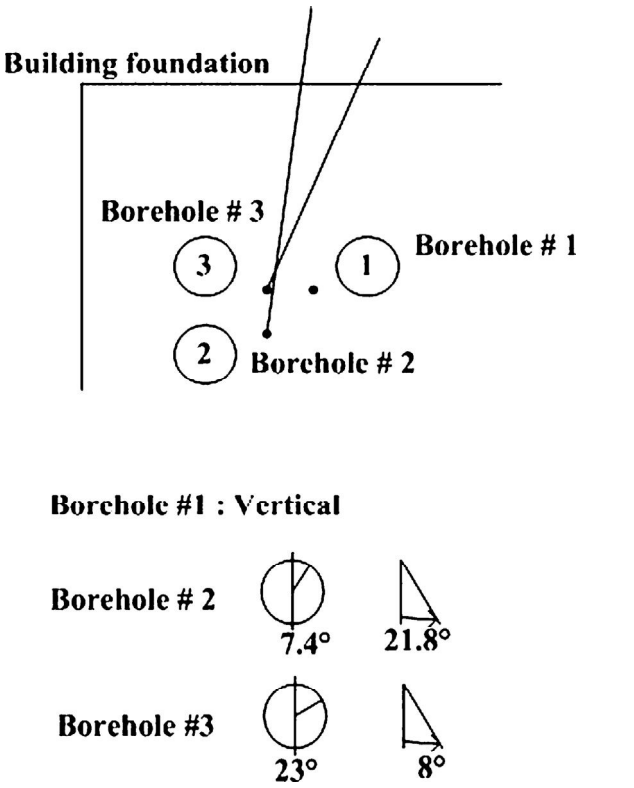

Fig. 3. Configuration of geothermal boreholes.

- Each evaporator had its expansion valve against one valve for the experimental device of Wang X. [16]. In addition, each liquid line was connected to each expansion valve with a hose end quickly ensuring equalization of pressure at the compressor stop.
- The refrigerant used in this study was R22.
- The test was carried out over a period of 30 days in early spring.

The objective of this study is to provide the scientific community with relevant information on the DX heat pump technology in order to facilitate its understanding and design.

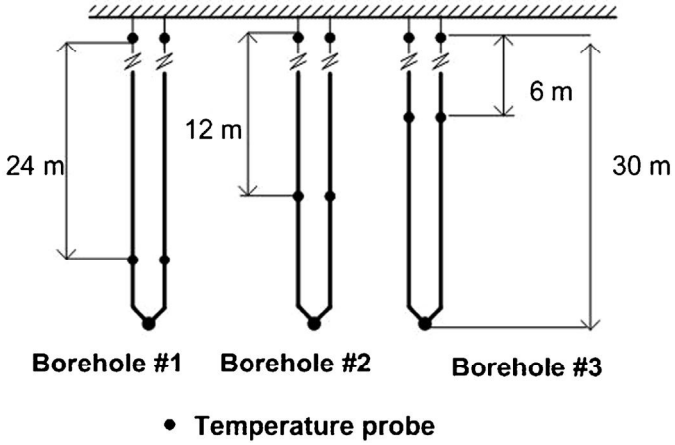

Fig. 4. Instrumentation of underground exchangers.

2. Description of the experimental setup and operation

2.1. Description of the experimental setup

The direct expansion geothermal heat pump used in this study is a unit model DXWG-45 by the Maritime Geothermal Company (Fig. 5). This reversible heat pump has a nominal cooling capacity of 10 kW and uses the R-22 (chlorodifluoromethane) fluid as a refrigerant. The device has a heat exchanger with coaxial water-refrigerant pipes (Turbotec BTSSC-60) on the inner side of the building (Laboratory) and a heat exchanger-ground heat refrigerant which comprises three parallel loops inserted in 30 m geothermal wells into the ground. Each loop has also an additional length of 20 m inside the building such that their total length was 50 m. Each loop consists of a copper tube with a 12.7 mm soft diameter and a soft copper tubing 9.7 mm in diameter. The two tubes are welded together at one of their ends, forming a U-tube (Fig. 6). The AC compressor piston, type (Tecumseh AVA5538EXN) has a rated power of 2.24 kW. Depending on the mode of operation of the system, expansion valves used differ: in cooling mode, a single expansion valve: TXV cooling (Fig. 5) (model Parker SE5VX100) with a 17.0 kW nominal capacity is used, while in heating mode, three expansion valves TXV heating (Fig. 5) (model Danfoss TUBE 068U2162) with a 2.6 kW nominal capacity each are used.

2.2. System operation

For the studied system, components and control strategies depend on the selected operating mode, and thus, the number of geothermal loops used in the two operating modes is different. Since the dimensions of the condenser and the evaporator (ground heat exchanger) differ significantly, it is difficult to manage refrigerant charge for the two operating modes. Indeed, the density of the refrigerant being generally higher during condensation at high pressure than during evaporation at low pressure, the control strategy is to limit to two the number of geothermal loops simultaneously activated during the operation of the system in cooling mode. This will allow the system to operate with a single refrigerant charge while maintaining satisfactory operation of a pressure refrigerant cycle for the two modes of operation. In addition, any excess refrigerant can be stored in the accumulator as dictated by operating conditions. Managing the refrigerant charge or size of the proposed heat exchangers in this fashion does not usually pose a problem with a classic secondary loop geothermal heat pump since the dimensions of the two heat exchangers in such a system are similar, and the accumulator suction is used to manage excess refrigerant when necessary. The total refrigerant charge in the system is 6.8 kg.

2.2.1. Operating in cooling mode

When the heat pump is operating in cooling mode, the integrated system control selects the number of geothermal loops to activate, depending on operating conditions and data recorded during the operation of the system (number of hours of use of each loop). The recovery lines of non-activated loops are used to get their coolant and allow the system to operate with a total refrigerant charge. Coolant flows to geothermal loops by three-way valves activated, is condensed and relaxed in the thermostatic expansion valve. Check valves prevent refrigerant flow through the heating expansion valves. Also, the heating valve is closed in cooling mode and to prevent the coolant from flowing through the collector liquid refrigerant used in this mode. During normal system operation, loops are activated in the following sequence: Loop #1, Loop #2, Loop #3, Loops #1 and #2, Loops #1 and #3, Loops #2 and #3. The system changes the control loop when the upper pressure of the refrigeration cycle

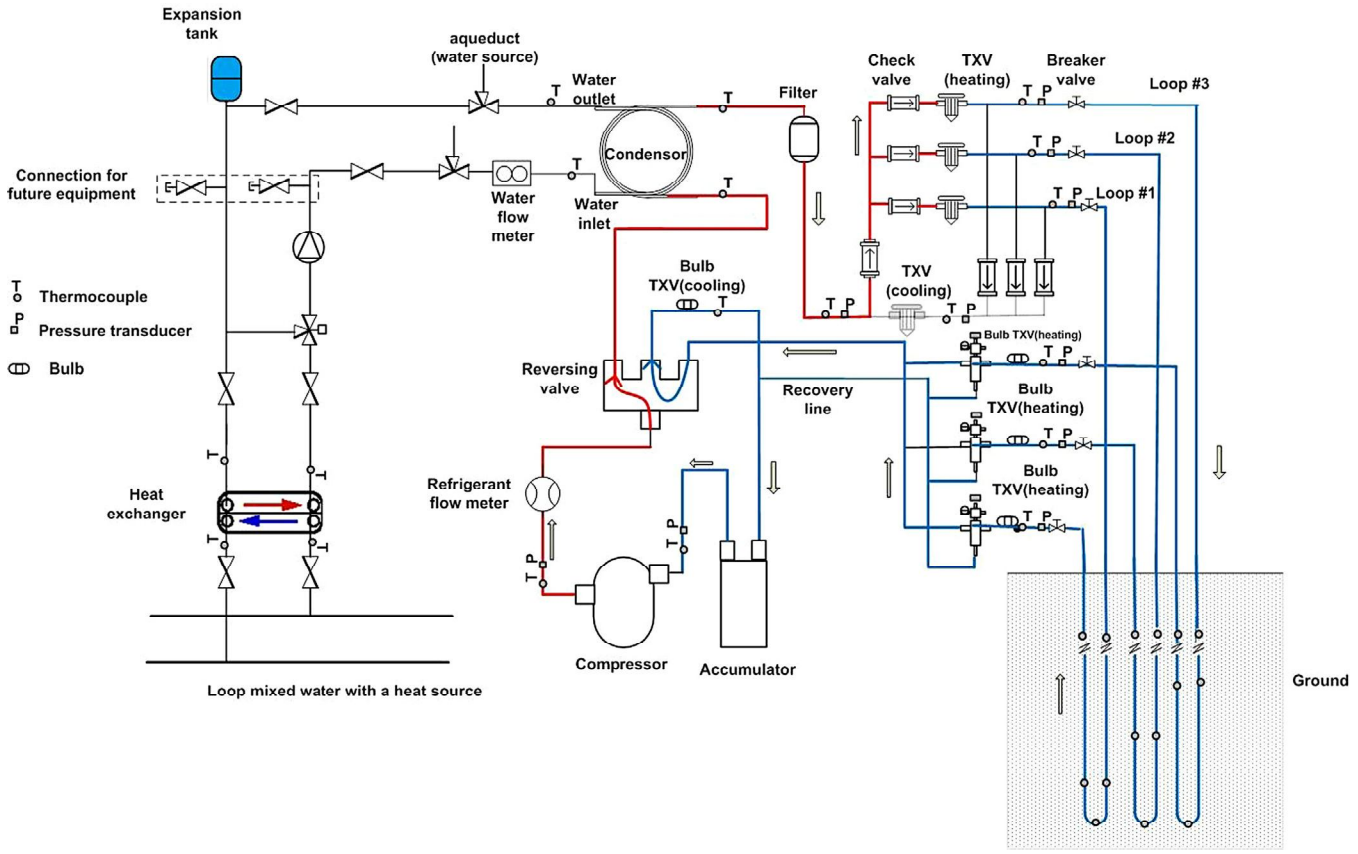

Fig. 5. Schematic of the experimental device in heating mode.

reaches about 2150 kPa. Thus, during operation of the air conditioning system, the condenser refrigerant heat exchanger basement which can be either a single loop or of two parallel loops does something.

2.2.2. System operation in heating mode

In heating mode, the three loops of the geothermal heat exchanger are activated and the flow of refrigerant is regulated in each loop by a thermostatic expansion valve. The check valves located downstream of the expansion valve dedicated to cooling mode prevent the refrigerant from flowing into this body. At the outlet of the condenser (water-refrigerant heat exchanger) the refrigerant is expanded through three thermostatic expansion valves connected in parallel (Fig. 5). The low-pressure refrigerant then evaporates in geothermal loops and flows through the three-way valves (not activated) to the accumulator (see Fig. 5). Thus, during operation of the heating system, the evaporator is a refrigerant-to-ground exchanger with three parallel loops which

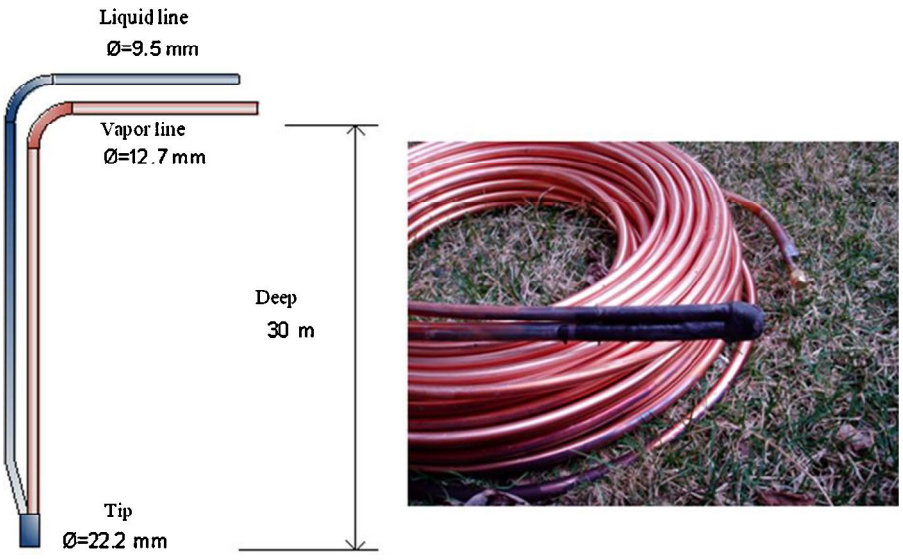

Fig. 6. Schematic of the U-tube.

are independently controlled by a thermostatic expansion valve dedicated to each loop.

3. Experimental methodology

The test campaign took place in early spring, going from April 03 to May 2, 2013, representing 30 days of continuous testing in heating mode. The schedule, which replaced operation of the heat pump each day, went from 8 am to 6 pm, for a total of 300 h of operation. The heat pump was thus in operation for 10 h a day, and stopped for 14 h. During the test, system data were recorded every 50 s. At the heat pump stop, the data acquisition system continued to operate until the next start of the heat pump. The goal here was to have the data needed to analyze the return to initial soil conditions and problems encountered when starting the compressor every day. Temperature sensors and pressure sensors properly calibrated installed in the circuit are shown in Figs. 4 and 5. The entire control system, as well as data acquisition and recording were managed in the Labview software environment.

4. Data reduction and uncertainty analysis

Heating capacity of condenser

$$Q_H = \dot{m}_w Cp_w (T_{w\_out} - T_{w\_in}) \quad (1)$$

Cp_w is taken constant.

Heat extraction rate from ground evaporator

$$q = \frac{Q_H - W_{Comp}}{3H} \quad (2)$$

COP_{hp} of heat pump unit

$$COP_{hp} = \frac{Q_H}{W_{Comp}} \quad (3)$$

The method used to assess the combined uncertainties is the uncertainty propagation implementation used by Comakli et al., Mohanraj et al., Gunes et al., and Guo et al. [2,20–22]. For example, the uncertainty of Q_H is calculated as:

$$\Delta Q_H^2 = \left(\frac{\partial Q_H}{\partial \dot{m}_w}\Delta \dot{m}_w\right)^2 + \left(\frac{\partial Q_H}{\partial T_{w\_out}}\Delta T_{w\_out}\right)^2 + \left(\frac{\partial Q_H}{\partial T_{w\_in}}\Delta T_{w\_in}\right)^2 + \left(\frac{\partial Q_H}{\partial Cp_w}\Delta Cp_w\right)^2 \quad (4)$$

where $\Delta\dot{m}_w$, ΔT_{w_out}, ΔT_{w_in}, ΔCp_w represent the uncertainty of its independent variables.

According to Table 1, for example,

$$\frac{\Delta \dot{m}_w}{\dot{m}_w} = \pm 1.50\% \quad (5)$$

$$\frac{\Delta T_{w\_out}}{T_{w\_out}} = \frac{\Delta T_{w\_in}}{T_{w\_in}} = \pm 0.40\% \quad (6)$$

The uncertainty for the calculated values are 4.10% for the heating capacity, 6.4% for the heat extraction rate in the soil, 4.60% for COP_{hp}, 0.10% for the evaporation temperature and condensation, 0.40% for superheating and 0.25% for the pressure drop in evaporation. The overall results of the standard uncertainties associated with each measured result of calibration certificates and those of derived quantities are presented in Table 1.

5. Results and discussion

On all graphs, if it is the date that is on the x-axis, the number 1 on the x-axis corresponds to the first day of practice, namely April 3, 2013; the number 2 corresponds to the second day, April 04, and so on until the number 30, which is the last day of testing corresponding to May 2, 2013. If it is the time that is on the x-axis, the value at each time represents the mean of the 30 (30 days) measurements that were taken at this time each day. For example, the value at 8:00 represents the mean of the 30 measurements that were taken at 8:00 O'clock each day.

Table 1
Daily average of the experimental and calculated values.

Items	Mean value	Unit	Uncertainty
Experimental mean value			
Condensation pressure	1419.97	kPa	±0.25%
Evaporation pressure in borehole #1	371.01	kPa	±0.25%
Evaporation pressure in borehole #2	370.41	kPa	±0.25%
Evaporation pressure in borehole #3	357.53	kPa	±0.25%
Condenser input temperature	32.00	°C	±0.40%
Heating water temperature	37.08	°C	±0.40%
Condenser water flow rate	0.38	$L\,s^{-1}$	±1.50%
Refrigerant flow rate	0.04	kg/s	±0.10%
Soil temperature in 30 m depth	13.22	°C	±0.40%
Heat pump unit power input	2.80	kW	±2.00%
Calculated value			
Heating capacity	8.04	kW	±4.1%
Evaporator heat extraction	5.24	kW	±6.4%
COP_{hp} of the heat pump unit	2.87	–	±4.6%
Evaporation temperature borehole #1	−8.61	°C	±0.10 °C
Evaporation temperature borehole #2	−8.65	°C	±0.10 °C
Evaporation temperature borehole #3	−8.20	°C	±0.10 °C
Condensation temperature	37.03	°C	±0.10 °C
Superheating borehole #1	6.94	°C	±0.40%
Superheating borehole #2	9.74	°C	±0.40%
Superheating borehole #3	12.03	°C	±0.40%
Pressure drop in borehole #1	217.81	kPa	±0.25%
Pressure drop in borehole #2	176.45	kPa	±0.25%
Pressure drop in borehole #3	187.49	kPa	±0.25%

Table 1 shows the average experimental and calculated values obtained during testing. According to the results, the average condensing pressure is 1419.97 kPa, which corresponds to a condensation temperature of about 37.03 °C for R22. During the tests, the power demand of the compressor was 2.8 kW at a compression ratio (ratio between the output pressure and inlet pressure of the compressor) of about 4.1. The heating capacity reached a daily average value of 8.04 kW. Lenarduzzi and Bennett [23] obtained a heating capacity of 8 kW for three wells each with a depth of 17 m, and each consisting of a copper tubing coiled spiral length of 122 m. Note that in our tests, the volumetric flow of cooling water remained constant at 0.38 $L\,s^{-1}$ (6 gpm). The average temperature of the heating water at the condenser outlet was around 37 °C when the average inlet temperature of the condenser water was 32 °C. These results are very encouraging for future DX heat pumps. Indeed, according to a report by the Canadian Department of Natural Resources on the development of energy efficiency in Canada from 1990 to 2009 [24], the average energy consumption of a residential home is 29,444.44 kWh per year, and the heating representing approximately 63%, or 18,550 kWh per year. The average month number of heating in Canada is about 7 months [25], the system presented in this study could provide an average of about 16,884 kWh per year or 91% of the national mean value only for 10 h use par day. Similarly, in Canadian environment, for example, according to data provided by M. Gervais et al. [26] relating to heating of 866 residential houses in a municipality in Quebec (Canada) where 538 houses have a maximum heating demand load between 6 kW and 8.6 kW with an average floor area ranging between 109 m^2 and 127 m^2. The DX heat pump presented in this study is able to cover between 93.5% and 100% of the peak load of the heating demand for the 538 houses in this municipality. Generally, it is recommended for maximum cost-effectiveness that the ground-source heat pumps should be sized to meet 60–70% of the total maximum demand load (the total space heating and

Table 2
Comparative electric heating and DX heat pump study.

Item	DX Heat pump	Electricity
Heating demand (kW)	8.04	8.04
Time heating per day (h)	10.00	10.00
Consumption per year (kWh)	16,884.00	16,884.00
Energy paid per year (kWh)	5040.00	16,884.00
Cost ($)	372.21	1248.66

water) [27]. This performance of the DX system is in agreement with the conclusion of Lund et al. cited by Ozgener et al. [28] that the geothermal heat pump have the largest installed capacity. From an economic point of view, Table 2 shows the economic performance of heating a dwelling house which the heating demand is 8.04 kW in two options: electrical heating and DX heat pump heating presented in this study for example. The results show that the choice of the DX heat pump would be very beneficial in that it offers cost savings of approximately 876.46 $, or about 70% per year. Costs are calculated based on residential electricity rates in Québec (the first 30 kWh are 0.0489$/kWh and each additional kWh is billed at 0.0740$).

Fig. 7 shows the mean values of the COP_{hp} and the refrigerant flow for 10 h, where the heat pump is working. COP_{hp} values obtained ranged from 2.70 to 3.44, with an overall average of about 2.87 per day. The average flow of refrigerant per day is about 0.04 kg/s. By comparison with a similar DX system, Lenarduzzi [23] obtained an average coefficient of performance of 2.85. Compared with the R22 SL systems used, Madani [29] obtained for the 200 m deep SL system a COP_{hp} of 2.52 for the same heating capacity of 8.04 kW. The SL system directed by Doherty et al. [30] consists of an 18-m deep well with a COP_{hp} of about 2.6. The COP_{hp} of Kara's SL system used R134a [31] consisting of a 55-m deep well, was 2.57. These values indicate that the DX system presented in this study is 12.2% more efficient than the Madani SL system, 9.4% more efficient than Doherty's system, and approximately 10.4% more efficient than the SL system as implemented by Kara. It can be concluded that in addition to saving money on the initial costs by removing the pump and the heat exchanger (see Figs. 1 and 2), DX systems are more efficient than SL systems. Note that during the winter months, the soil temperature was between 12 °C and 17 °C and seasonal COP_{hp} between 2.7 and 3.6.

Fig. 8 reflects the mean values of the heating capacity, power demand by the compressor and COP_{hp} when the heat pump is working. From this Figure, the time trend seen indicates that the mean heating capacity decreased slightly throughout the day, from 8.14 kW at 11 h (early steady state) to 7.84 kW at 6:00 pm.

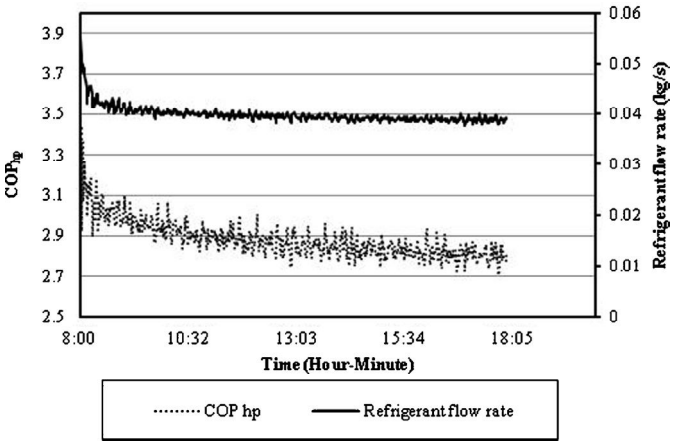

Fig. 7. Hourly performance coefficient and refrigerant flow average.

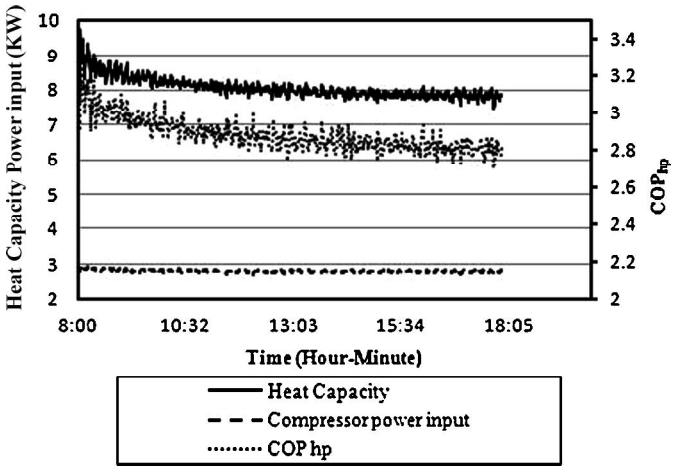

Fig. 8. Hourly heating capacity, power consumption and COP_{hp} average.

It represents an average decrease of 3.7%. Similarly, the mean power demand by the compressor decreased from 2.8 kW to 2.7 kW (about 3.6%) and the mean COP_{hp} decreased from 2.87 to 2.80 (about 2.4%). Lenarduzzi et al. [23] obtained the heating capacity decrease of 12% and the COP dropped about 14% for its DX heat pump.

Fig. 9 shows the variations in daily average of the temperature of heating water (outlet condenser), outdoor temperature and COP_{hp} of the DX heat pump unit during the tests. Based on observations, the heating water temperature is practically constant despite large variations in the outside temperature. Similarly, the COP_{hp} varies between 2.92 and 2.83 with an average of 2.87 and a standard deviation about 0.6% (lower value). We can conclude that outside temperature does not have any practical negative influence on the performance of the DX heat pump, which confirms its advantage on air to air heat pumps where performance decreases with a decrease of outdoor temperature [32] because it is unable to load to air source, the heat needed to evaporate the refrigerant.

Once the DX heat pump is installed, the parameters that could influence the performance of the DX heat pump side of the building are: the inlet temperature, the flow of cooling water to the condenser, and the time of use. Fig. 10 shows the variations of daily average of: (i) the condenser water inlet temperature, (ii) the condensing temperature, (iii) the coefficient of performance of the DX heat pump. The results show that when the inlet cooling water temperature increases, the condensation temperature of the refrig-

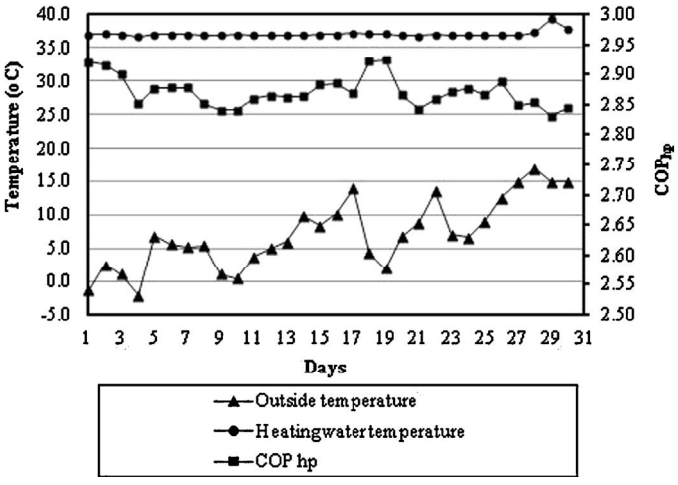

Fig. 9. Daily average of outside air temperature, heating water temperature and COP_{hp}.

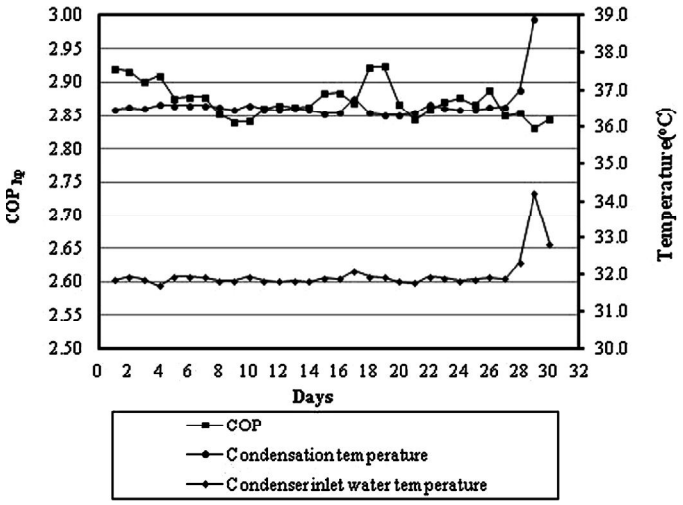

Fig. 10. Daily average of condenser inlet water temperature and COP_{hp}.

erant increases as well. Indeed, an increase in the inlet temperature reduces the cooling of the refrigerant to the condenser, leading to an increase in the condensation temperature and the COP_{hp} decreases. So the performance of the heat pump decreases. To confirm this conclusion, additional tests were performed to vary the condenser water inlet temperature during the working of DX heat pump. Fig. 11 shows the results of tests carried out about one hour after the steady state was established. This figure shows that when the cooling water temperature increases, the performance of the system decreases, and the best performances of the DX system presented in this study are obtained for cooling water temperatures below 35 °C.

For all the 30 days of testing, the cooling water flow was kept constant. To provide an understanding of how to vary the coefficient of performance and the heating capacity of the DX system dependent on the cooling water flow rate through the condenser, additional tests were also carried out. The test performed consisted in operating the heat pump when the steady state is reached, for a period of 30 min for each condenser cooling water flow rate value before moving to the next value. The values of COP_{hp} and of Q_H for this flow rate value were the average of the measured values during the 30 min working. Fig. 12 shows the variations of COP_{hp} and Q_H versus cooling water flow to the condenser. According to this figure, it can be concluded that the COP_{hp} and the heating capacity of the DX heat pump increase when the cooling water flow increases, but what is interesting is that the shape of the curves allows us

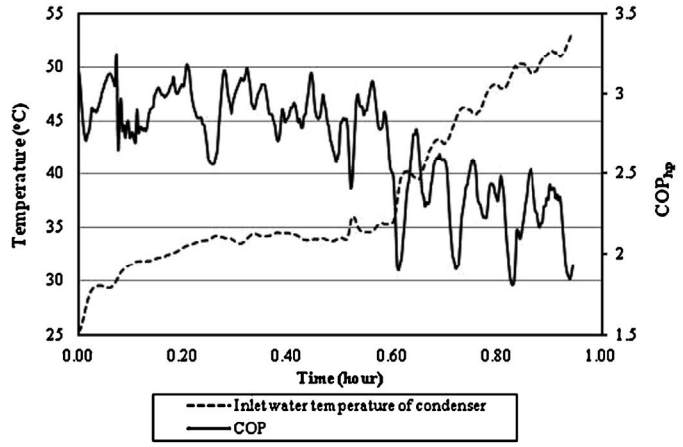

Fig. 11. Inlet cooling water temperature of condenser and COP_{hp}.

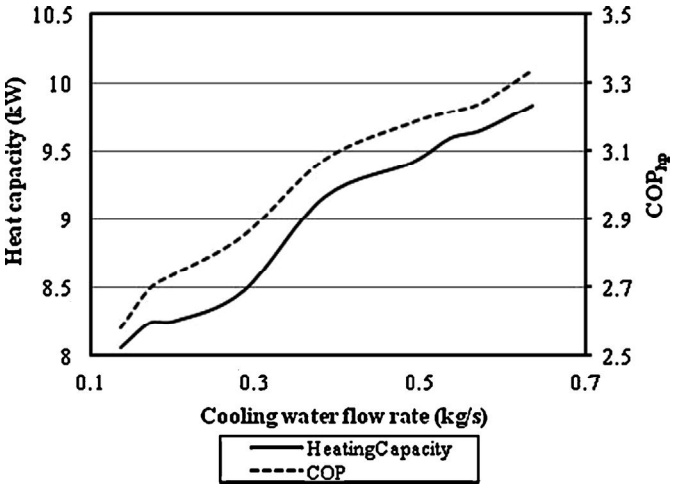

Fig. 12. Variations of the heating capacity and COP_{hp} vs. flow rate of the cooling water.

to find a correlation between the COP_{hp} and Q_H and the cooling water flow rate. Thus, regression analyses of the COP_{hp} and the heating capacity as a function of the condenser cooling water flow rate were performed with correlation coefficients in the range of 99.99% for the COP_{hp} and 99.87% for the heating capacity Q_H. Eqs. (7) and (8) obtained the simplified regression models that can be used for feasibility studies of the design of the DX heat pump in similar conditions.

$$COP_{hp} = -2103.2\dot{m}_e^6 + 5188.9\dot{m}_e^5 - 5086.3\dot{m}_e^4 + 2515.6\dot{m}_e^3 - 657.93\dot{m}_e^2 + 87.6\dot{m}_e - 1.98 \quad (7)$$

$$Q_H = -8950\dot{m}_w^6 + 21293\dot{m}_w^5 - 20136\dot{m}_w^4 + 9594\dot{m}_w^3 - 2403.2\dot{m}_w^2 + 301.11\dot{m}_w - 6.62 \quad (8)$$

Fig. 13 shows the variations of the condensing temperature and the COP_{hp} versus cooling water flow to the condenser. According to this figure, although the condensing temperature varies greatly depending on the flow rate, the COP_{hp} increases due that the heating capacity increases with the flow rate of cooling water and the power consumed by the compressor varies little. Therefore we can observe in Fig. 13 three different zones. For low flow rate (flow rate between 0.13 L s^{-1} and 0.29 L s^{-1}), the coefficients of performance of the DX heat pump remain relatively low. In the second

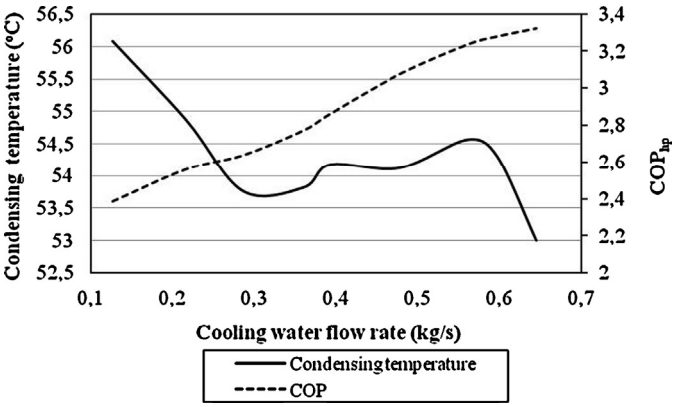

Fig. 13. Variations of the condensing temperature and COP_{hp} vs. flow rate of the cooling water.

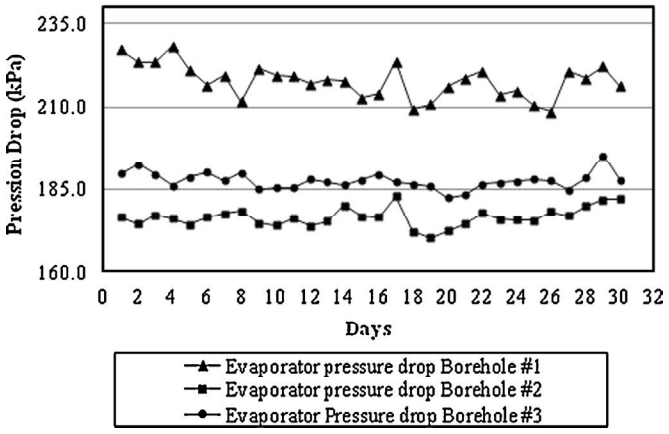

Fig. 14. Variations of daily average pressure drop in the evaporators.

zone (flow rate between 0.29 L s^{-1} and 0.56 L s^{-1}) the condensing temperature remain almost stable and the performance generally increases slightly with small variations. Finally the high flow rate (flow rate greater than 0.56 L s^{-1}) area where the condensing temperature decreases quickly and the COP_{hp} reach the highest values. It can be concluded that, in general, when increasing the cooling water flow rate, the condensing temperature drops and a minimum of cooling water flow rate is necessary to ensure proper operation of the DX heat pump and avoid reaching the condensing pressure very high. In this study the minimum value of the volumetric flow rate is about 0.13 L s^{-1}. A regression analysis is also performed. The relation (9) shows the result obtained with a correlation coefficient of 99.03%.

$$T_{cd} = -28286\dot{m}_w^6 + 66746\dot{m}_w^5 - 63255\dot{m}_w^4 + 30512\dot{m}_w^3 - 7774.7\dot{m}_w^2 + 965.74\dot{m}_w + 10.714 \quad (9)$$

Another factor limiting the performance of DX heat pumps is the drop in the ground heat exchanger (evaporator). Indeed, a significant pressure drop in the soil causes a decrease in pressure and temperature evaporation, causing the compressor to consume more energy to meet the high pressure. The compression ratio is therefore raised, without exceeding the limit of 6 in order to avoid damaging the compressor. From Eq. (3), COP_{hp} therefore decreases. In this study, the average rate of compression achieved is 4.1. Fig. 14 shows the average daily pressure drop in the three evaporators. The averages are 217.8 kPa for borehole #1, 176.4 kPa for borehole #2 and 187.5 kPa in borehole #3. We deduce that the average pressure drop per evaporator is 194 kPa for an average evaporator inlet pressure of 564.4 kPa. It represents approximately 34.4%. This drop is equivalent to 1.93 kPa m^{-1} of the total length of the geothermal loop. Lenarduzzi et al. [23] obtained a pressure drop of 1.13 kPa m^{-1} with R22 used as refrigerant in a 122 m loop. Wang X. et al. [16] obtained a 160 kPa drop with a DX heat pump of the same length and the same configuration loop as that presented in this study, but with a different refrigerant (R134a) configuration.

Fig. 15 shows the variations of the daily average pressure drop in geothermal evaporators and the coefficient of performance of the DX heat pump. It can be noted that when the pressure drop increases, the COP_{hp} decreases. In other words, if the pressure drop is low, the compressor consumes less energy, and the system is more efficient.

As shown above, the technology used for the loop configuration in this study is in heating mode, and each loop has its own thermostatic expansion valve (Fig. 5), essentially favoring a significant control of refrigerant flow in each evaporator. Fig. 16 shows the superheating value calculated at the output of each evaporator.

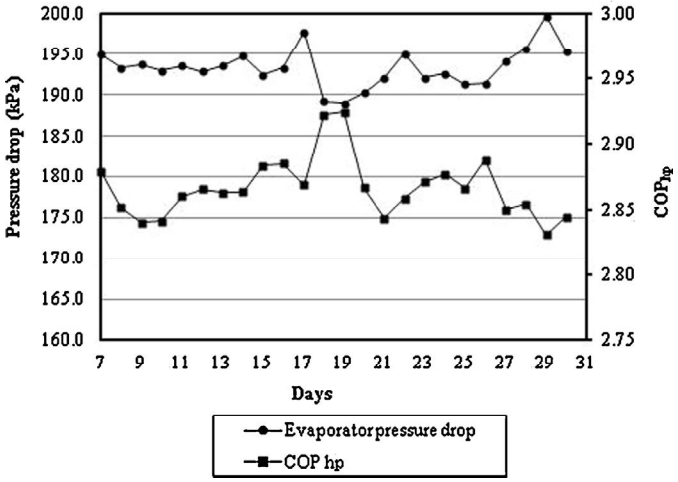

Fig. 15. Daily average pressure drop in the evaporator and COP_{hp}.

Based on these results, the average superheating calculated in loops #1, #2, #3 is respectively 7 °C, 9.7 °C and 12 °C. In the case of the conventional heat pump, the acceptable limit is 4–7 °C. In this study, only the first value is within limits. The others superheating values are way above the permissible values. Suggesting that just a little refrigerant flow rate passes through the expansion valves installed on loops #2 and #3.

We then deduce a mal-distribution of flow through the evaporator, causing instabilities at the pressures at the inlet evaporators #2 and #3. This is manifested by oscillations of pressures and temperatures at the inlet of the evaporators (see Figs. 17 and 18). Wang X. used a DX technology with one thermostatic expansion valve and obtained the same result. However, this behavior does not affect the overall operation of the DX heat pump because the refrigerant charge required is sucked to compressor with superheating between 1.4 °C and 2.1 °C (see Fig. 16). As can be seen, this suction superheat is lower than usual and we observe a large temperature drop between the exit of the boreholes and the entrance of the compressor. This temperature drop could not be explained by a simple pressure drop since the measured pressure at the compressor inlet is almost the same as the one at the evaporator manifold. We believe that a possible evaporation of some liquid in the accumulator can be responsible for this temperature drop. It is not clear for us why such liquid remains after several hours of operation and

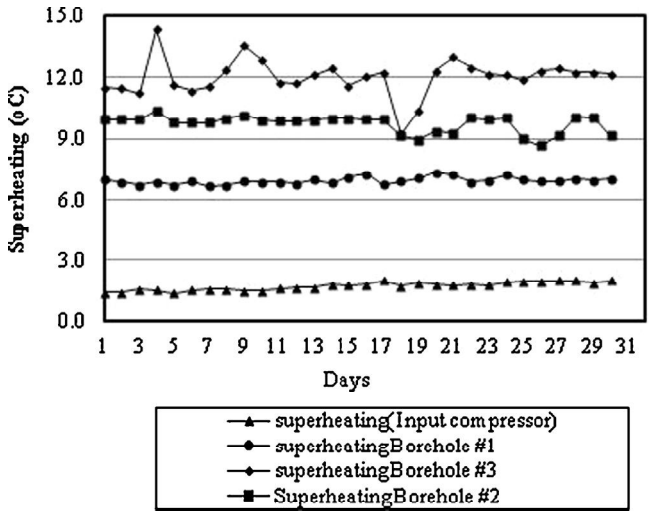

Fig. 16. Evaporator outlet superheating.

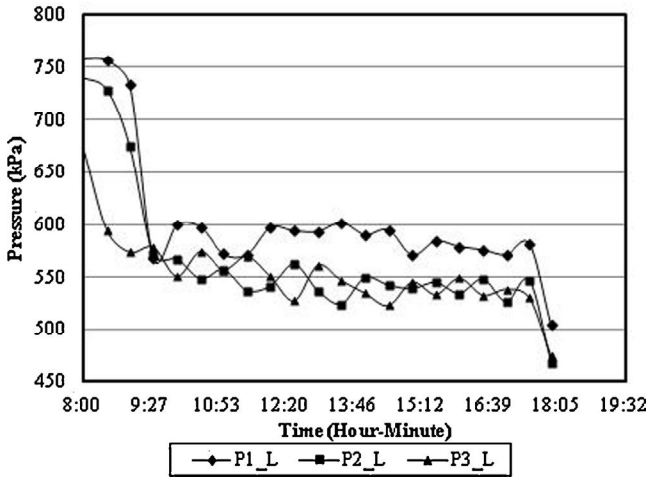

Fig. 17. Evaporator inlet pressure.

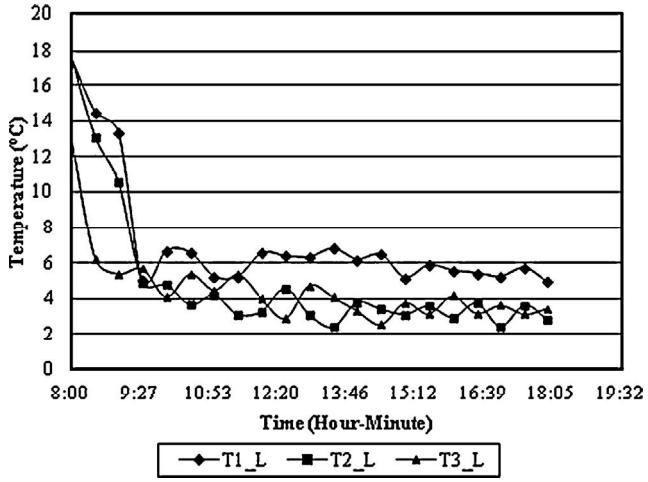

Fig. 18. Evaporator inlet temperature.

this will be the scope of a future study. The condenser subcooling in this study is around 1 °C.

In this study, we did not have any difficulty of starting the compressor due to oil return problem raised by Mei et al. and Wang et al. [11,17]. Figs. 19–20 show the variations of the inlet pressure and the inlet temperature of the compressor when the system is stopped.

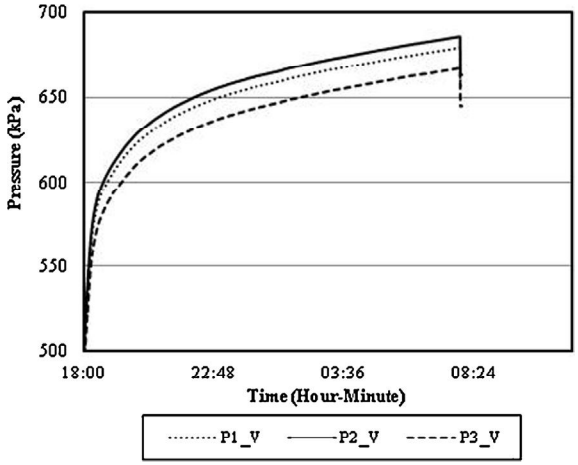

Fig. 19. Variations of vapor line pressure when the compressor stops.

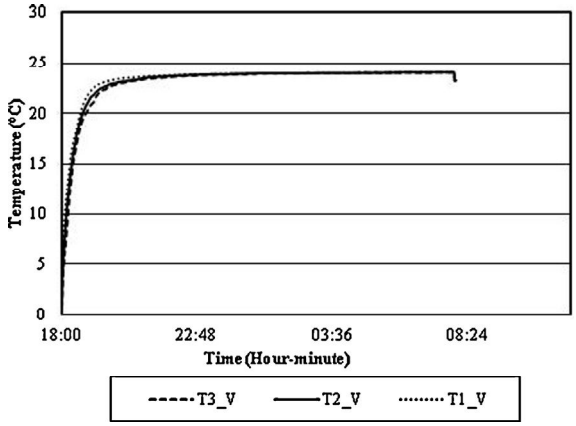

Fig. 20. Variations of vapor line temperature when the compressor stops.

According to [11], a rapid increase in pressures and temperatures is due to a migration of the refrigerant from the accumulator. The wells are filled with refrigerant in two-phase state, and as a result, the gravitational force deployed by the compressor at startup is thus minimized. Therefore, the system starts normally after each stop of the compressor. It should be noted that to resolve the oil return problem, Wang et al. [17] had to install a circular ring at the mid-height level of the refrigerant circuit inside the geothermal wells, and trap much of the lubrication oil, preventing it from penetrating the pit. This device although, wanting address the question of lubricating oil return may cause additional pressure drop in the evaporator due to the circular geometry is not necessary in the experimental device presented in this study.

Fig. 21 shows the average soil temperature at 30 m in contact with the evaporator tube at system startup. The daily average temperature value of the soil in contact with the ground when the compressor starts is 13.2 °C. On the first day (April 3, 2013), the temperature at this point is 14.6 °C, while on the last day of testing, May 2, 2013, this value changes to 13.5 °C, which corresponds to an average cooling of 1.1 °C for 300 h of operation, and represents a decrease of approximately 7.5%. We see that despite the 14-h shutdown, the ground contacting the U-tube does not fully return to its original conditions because of the heat that is extracted. The average value of the heat extracted from the ground in this study is 5.24 kW (see Table 1), and the corresponding heat extraction rate is 58.2 W m^{-1}. Wang X. et al. [16] in their study found 51.5 W m^{-1}, and Wang H. et al. [17] obtained 54.4 W m^{-1}. The heat extraction rate is a very specific parameter in the design of DX heat pumps. Percebois [33], in his book on the geothermal heating recommends, for the design of a DX heat pump on ground covered with saturated gravel or sand, a heat extraction rate ranging from 55 to 65 W m^{-1}

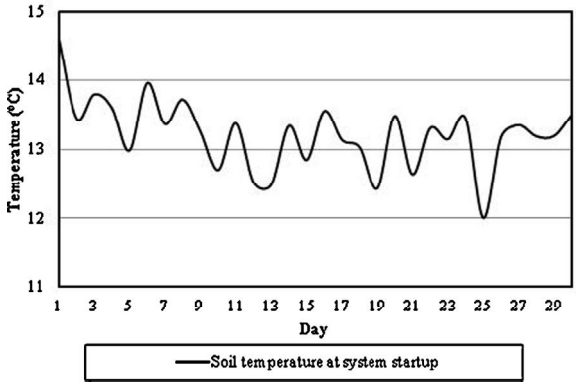

Fig. 21. Daily average soil temperature at 30 m.

for 2400 h of use per year and 65 to 80 W m^{-1} for 1800 h of use per year. Similarly, the European standard EN 15450 Heating System in Buildings-Design of Heat Pump Systems, recommends an extraction rate of 50–60 W m^{-1} for sizing a DX heat pump installed in a water-saturated sediment when the hours of use fall between 1800 and 2400 h. As secondary loops for the geothermal heat pumps, they provide heat extraction rates of between 25 and 35 W m^{-1} for a single U-tube, and 35 and 45 W m^{-1} for two U-tubes [6,34]. By comparison, the DX heat pumps offer the best heat transfer, which has the effect of reducing the well depth, and therefore the cost of drilling.

The heat extraction rate depends, among other things, on the thermal properties of the soil and grout (thermal conductivity and thermal diffusivity). In other words, the heat extraction rate varies depending on the model chosen to characterize the thermal resistance of the heat transfer between the ground and the refrigerant. Lamarche [35], in carrying out a comparative study of different methods of assessing the thermal resistance approaches, proposed best practices and analyzed the impact of different methods on the design of the ground heat exchanger. More specifically, Spilker [36] analyzed the influence of different materials on the embankment design of geothermal heat exchangers, and concluded that the length of a geothermal heat exchanger can be reduced by using sand or thermally improved bentonite grout instead of standard bentonite grout. Similarly, Mei [37] tested three backfill materials: clay, sand, and a fluidized mixture used for backfilling of underground cable. The results indicated that the filler affects the performance of the geothermal heat exchanger; the fluidized mixture dissipates 47% more heat than clay and 23% more than the sand.

Ideally, the DX heat pump should be used in balanced mode: heat should be drawn from the ground in the winter and heat stored in the summer. This would avoid exhausting the soil after several years of use because geothermal systems are designed for a service life of 25–30 years.

6. Conclusion

At the end of this experimental investigation, we can conclude that:

- Direct expansion heat pump technology is feasible and it works very well in on-off mode.
- The system makes it possible to reach a daily average heating capacity of 8.04 kW, and an average coefficient of performance of 2.87. The maximum value of COP_{hp} is 3.44.
- The choice of the DX heat pump as a source of residential heating is very beneficial, providing net savings of around 70% compared to electricity.
- The heat extraction rate obtained from the soil in the DX GHP is better than those of SL GHP, which in terms of sizing, are more economical for DX heat pump by reducing the borehole length. In this study, it is 58.2 W m^{-1}.
- The performance of the system decreases when the cooling water temperature of the condenser increases, and the best performances of the DX system presented in this study are obtained for cooling water temperatures below 35 °C.
- In DX systems, dimensioning efforts should be made to minimize pressure drop in the evaporator in order to find a compromise between low pressure drop, oil return and refrigerant charge. For example, an increase in the diameter of the U-tube can reduce the pressure drop but increase the refrigerant charge and the difficulty of oil return to the compressor.
- In geothermal loops in parallel, the flow distribution could be uneven. The installation of the flow rate balancing valves might help improve this situation. This approach will be explored in our future studies.
- Demonstrated performance and savings engendered by the DX heat pump prove that such pumps represent a good alternative to the secondary loop and air–air heat pumps for residential heating.

Research currently underway in our laboratory will allow short-term to a comprehensive simulation model of a DX heat pump, facilitating further analysis to provide the tools necessary to design the operating and test performance of DX systems using refrigerants such as R407C and R410A, which are the refrigerant alternatives to R22 in the area of heat pumps.

Acknowledgements

Financial support for this study was provided by Canadian Department of Natural Resources (Canmet Energy), École de technologie supérieure and its financial partners; the authors would like gratefully to acknowledge their invaluable contributions. In addition, the valuable comments of the reviewers are gratefully acknowledged.

References

[1] K. Raffety, Geothermal heat pump systems: an introduction, Water Well Journal 57 (8) (2003) 24–28.
[2] Y. Guo, G. Zhang, J. Zhou, J. Wu, W. Shen, A techno-economic comparison of a direct expansion ground-source and a secondary loop ground-coupled heat pump system for cooling in a residential building, Applied Thermal Engineering 35 (2012) 29–39.
[3] S.J. Self, B.V. Reddy, M.A. Rosen, Geothermal heat pump systems: status review and comparison with other heating options, Applied Energy 101 (2013) 341–348.
[4] J. Lund, Ground-source (geothermal) heat pumps, in: P.J. Lineau (Ed.), Course on Heating with Geothermal Energy: Conventional and New Schemes. World Geothermal Congress 2000 Short Courses, Kazuno, Tohuko District, Japan, 2000, pp. 209–236.
[5] A. Capozza, M. De Carli, A. Zarrella, Design of borehole heat exchangers for ground-source heat pumps: a literature review, methodology comparison and analysis on the penalty temperature, Energy and Buildings 55 (2012) 369–379.
[6] H. Wang, C. Qi, H. Du, J. Gu, Thermal performance of borehole heat exchanger under groundwater flow: a case study from Baoding, Energy and Buildings 41 (12) (2009) 1368–1373.
[7] C. Montagud, J.M. Corberán, Á. Montero, J.F. Urchueguía, Analysis of the energy performance of a ground source heat pump system after five years of operation, Energy and Buildings 43 (12) (2011) 3618–3626.
[8] H. Esen, M. Inalli, Modelling of a vertical ground coupled heat pump system by using artificial neural networks, Expert Systems with Applications 36 (7) (2009) 10229–10238.
[9] A. Hepbasli, O. Akdemir, E. Hancioglu, Experimental study of a closed loop vertical ground source heat pump system, Energy Conversion and Management 44 (4) (2003) 527–548.
[10] H. Halozan, R. Rieberer, Ground source heat pumps – overcoming market and technical barriers, in: IEA Heat Pump Programme Annex 29, Zurich, 2008.
[11] Mei, Baxter, Experimental Analysis of Direct-Expansion Ground-Coupled Heat Pump Systems, Oak Ridge National Laboratory, Tennessee, 1991.
[12] Mei, Baxter, Experimental study of direct-expansion ground coil heat exchangers, in: Ashrae Transaction, Vol. 96, no. 1, 1990, pp. 821–825.
[13] B. Beauchamp, L. Lamarche, S. Kajl, Experimental evaluation of a direct expansion evaporator using multiple U-tube heat exchangers in parallel, in: VI^{ème} Colloque Interuviversitaire Franco-Québecois sur la Thermique des Systèmes, Krakow, Poland, 2009.
[14] B. Beauchamp, Modeling and experimental validation of a direct expansion geothermal heat pump Génie Mécanique (Ph.D. thesis), École de Technologie Supérieure, Université du Québec, 2011.
[15] P.J. Hughes, Geothermal (Ground-Source) Heat Pumps: Market Status, Barriers to Adoption, and Actions to Overcome Barriers, U.S.D.o.E. Oak Ridge National Laboratory, Office of Scientific and Technical Information, 2008, pp. 40.
[16] X. Wang, C. Ma, Y. Lu, An experimental study of a direct expansion ground-coupled heat pump system in heating mode, International Journal of Energy Research 33 (15) (2009) 1367–1383.
[17] H. Wang, Q. Zhao, J. Wu, B. Yang, Z. Chen, Experimental investigation on the operation performance of a direct expansion ground source heat pump system for space heating, Energy and Buildings 61 (2013) 349–355.
[18] B.T. Austin, K. Sumathy, Parametric study on the performance of a direct-expansion geothermal heat pump using carbon dioxide, Applied Thermal Engineering 31 (17–18) (2011) 3774–3782.

[19] C. Rousseau, J.-L. Fannou, L. Lamarche, S. Kajl, Modeling and analyse of a direct expansion geothermal heat pump (DX): part 1. Modeling of ground heat exchanger, in: COMSOL Conference, Boston, USA, 2012.
[20] M. Mohanraj, S. Jayaraj, C. Muraleedharan, Exergy assessment of a direct expansion solar-assisted heat pump working with R22 and R407C/LPG mixture, International Journal of Green Energy 7 (1) (2010) 65–83.
[21] S. Gunes, E. Manay, E. Senyigit, V.A. Ozceyhan, Taguchi approach for optimization of design parameters in a tube with coiled wire inserts, Applied Thermal Engineering 31 (14–15) (2011) 2568–2577.
[22] K. Comakli, F. Simsek, O. Comakli, B. Sahin, Determination of optimum working conditions R22 and R404A refrigerant mixtures in heat-pumps using Taguchi method, Applied Energy 86 (11) (2009) 2451–2458.
[23] F.J. Lenarduzzi, T.J. Bennett, A Direct-Expansion Ground-Source Heat Pump with Spiral Ground Coil-Heating Mode, in: Ashrae Transactions, Vol. 97, no. 1, New York, 1991.
[24] N.R. Canada, Energy Efficiency Trends in Canada 1990 to 2009, N.R.C.s.O.o.E. Efficiency, Natural Resources Canada's Office of Energy Efficiency, Canada, 2011, pp. 58.
[25] D. Phillips, The Climates of Canada, Environment Canada, Ottawa, Canada, 1990.
[26] M. Gervais, S. Kajl, C. Schweigler, J. Paris, Design and operating parameters of a district heating network, in: 8th Interuniversity Symposium France–Québec on Thermal Systems, Montréal, Canada, 2007, pp. 323–328.
[27] N.R. Canada, Heating and Cooling With a Heat Pump, N.R.C.s.O.o.E. Efficiency, Natural Resources Canada's Office of Energy Efficiency, Canada, 2004, pp. 55.
[28] O. Ozgener, A. Hepbasli, Modeling and performance evaluation of ground source (geothermal) heat pump systems, Energy and Buildings 39 (1) (2007) 66–75.
[29] H. Madani, J. Claesson, P. Lundqvist, Capacity control in ground source heat pump systems part II: comparative analysis between on/off controlled and variable capacity systems, International Journal of Refrigeration 34 (8) (2011) 1934–1942.
[30] P.S. Doherty, S. Al-Huthaili, S.B. Riffat, N. Abodahab, Ground source heat pump—description and preliminary results of the Eco House system, Applied Thermal Engineering 24 (17–18) (2004) 2627–2641.
[31] Y.A. Kara, Experimental performance evaluation of a closed-loop vertical ground source heat pump in the heating mode using energy analysis method, International Journal of Energy Research 31 (15) (2007) 1504–1516.
[32] S.P. Lohani, D. Schmidt, Comparison of energy and exergy analysis of fossil plant, ground and air source heat pump building heating system, Renewable Energy 35 (6) (2010) 1275–1282.
[33] J. Percebois, The Guide of Geothermal Heating, Eyrolles ed., 2011.
[34] X. Li, Y. Chen, Z. Chen, J. Zhao, Thermal performances of different types of underground heat exchangers, Energy and Buildings 38 (5) (2006) 543–547.
[35] L. Lamarche, S. Kajl, B. Beauchamp, A review of methods to evaluate borehole thermal resistances in geothermal heat-pump systems, Geothermics 39 (2) (2010) 187–200.
[36] E.H. Spilker, Ground-coupled heat pump loop design using thermal conductivity testing and the effect of different backfill materials on vertical bore length, in: Ashrae Transactions, Vol. 104, no. 1A, San Francisco, 1998.
[37] V.C. Mei, Effect of backfilling material on ground coil performance, in: Ashrae Transaction, Part 2, Toronto, 1998.